Supplementary Information (SI) for Green Chemistry.

Supporting Information for:

Platinum nanoparticle-doped recycled PLA filament for sustainable additive manufactured electrocatalytic architectures

Karen K. L. Augusto[1,2], Robert D. Crapnell[1], Elena Bernalte[1], Orlando Fatibello-Filho[2], and Craig E. Banks[1*]

[1]*Faculty of Science and Engineering, Manchester Metropolitan University, Dalton Building, Chester Street, M1 5GD, Great Britain.*
[2]*Laboratório de Analítica, Bioanalítica, Biosensores, Electroanalítica e Sensores, Departamento de Química, Universidade Federal de São Carlos (UFSCar), CP 676, 13560-970 São Carlos-SP, Brazil.*

*To whom correspondence should be addressed.

E-mail: c.banks@mmu.ac.uk; Tel: +44(0)1612471196

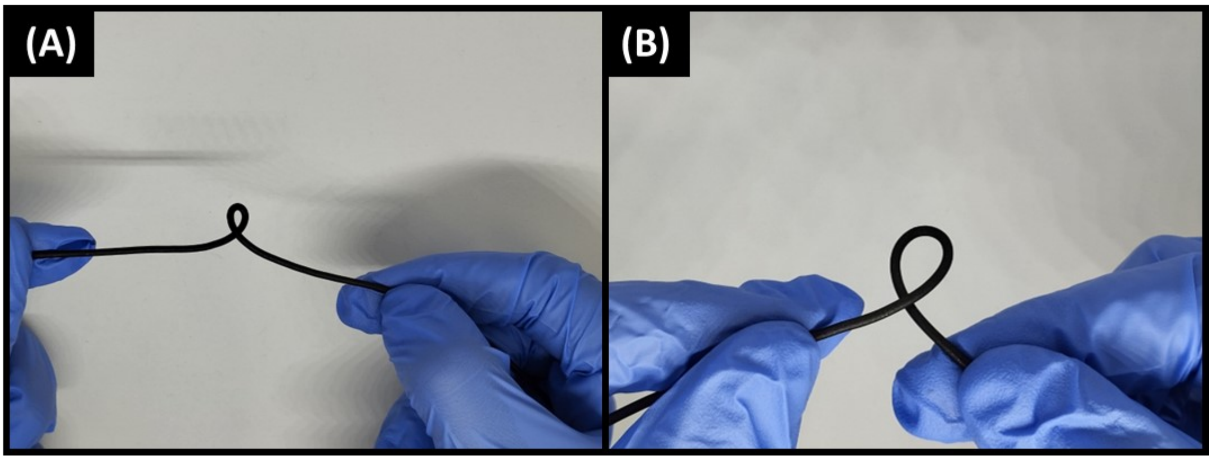

Figure S1. Image of the bespoke (A) graphite and (B) PtNPs-G filaments, highlighting the flexibility.

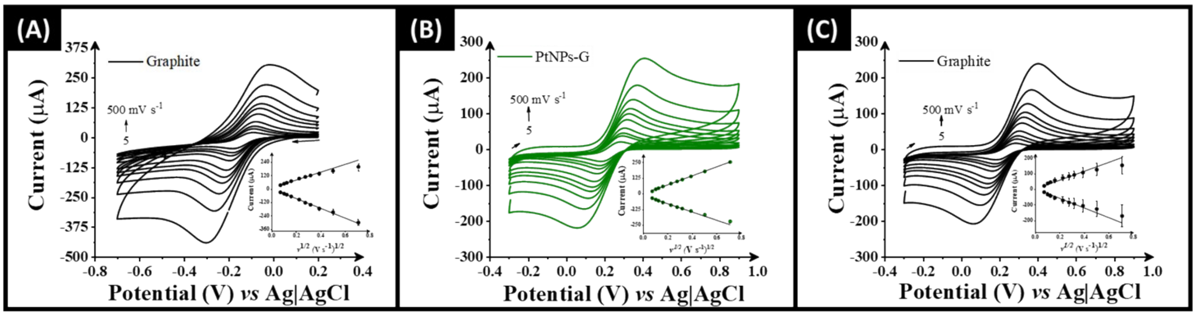

Figure S2. (A) Scan rate study (5 – 500 mV s^{-1}) with $[Ru(NH_3)_6]^{3+}$ (1 mM in 0.1 M KCl) performed in the graphite as the WE. Inset: the Randles–Ševčík plot. (B and C) Scan rate study (5 – 500 mV s^{-1}) with $[Fe(CN)_6]^{4-}$ (1 mM in 0.1 M KCl) performed in the PtNPs-G and graphite as the WE. Inset: the Randles–Ševčík plot.

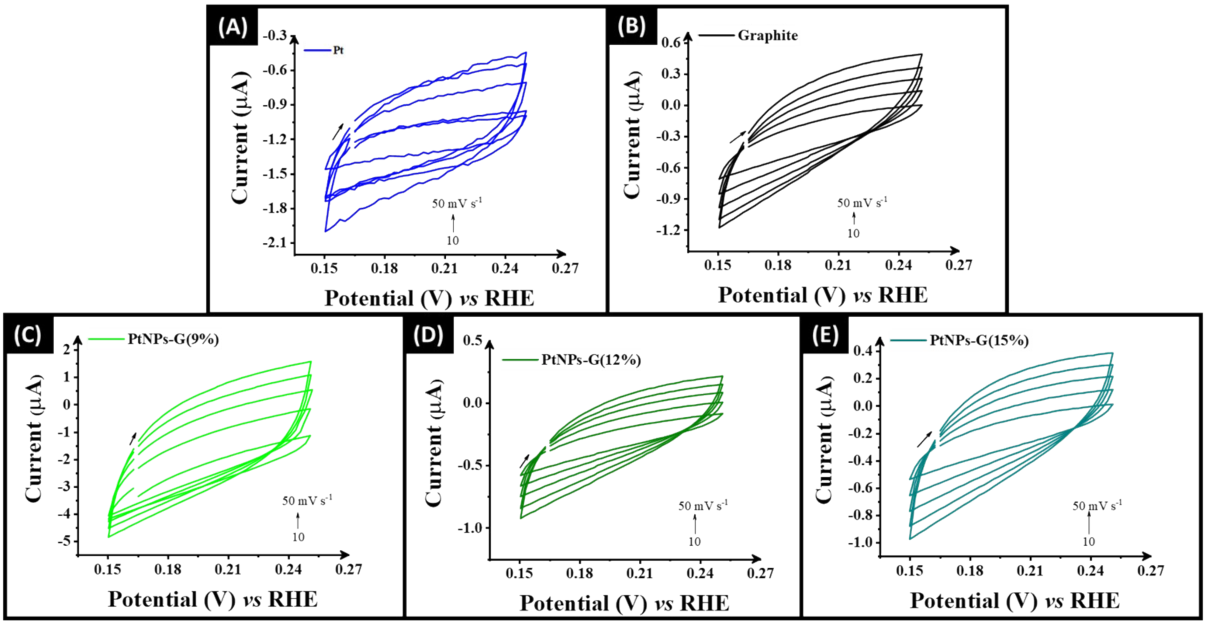

Figure S3. Cyclic voltammograms at non-Faradaic region (+0.15 to +0.25 V) at the following scan rates: 10, 20, 30, 40, and 50 mV s^{-1} with (A) polycrystalline platinum electrode, (B) Graphite and (C to E) electrodes with different amounts of PtNPs-G (9, 12, and 15%). Solution composition: 0.5 mol L^{-1} H_2SO_4.

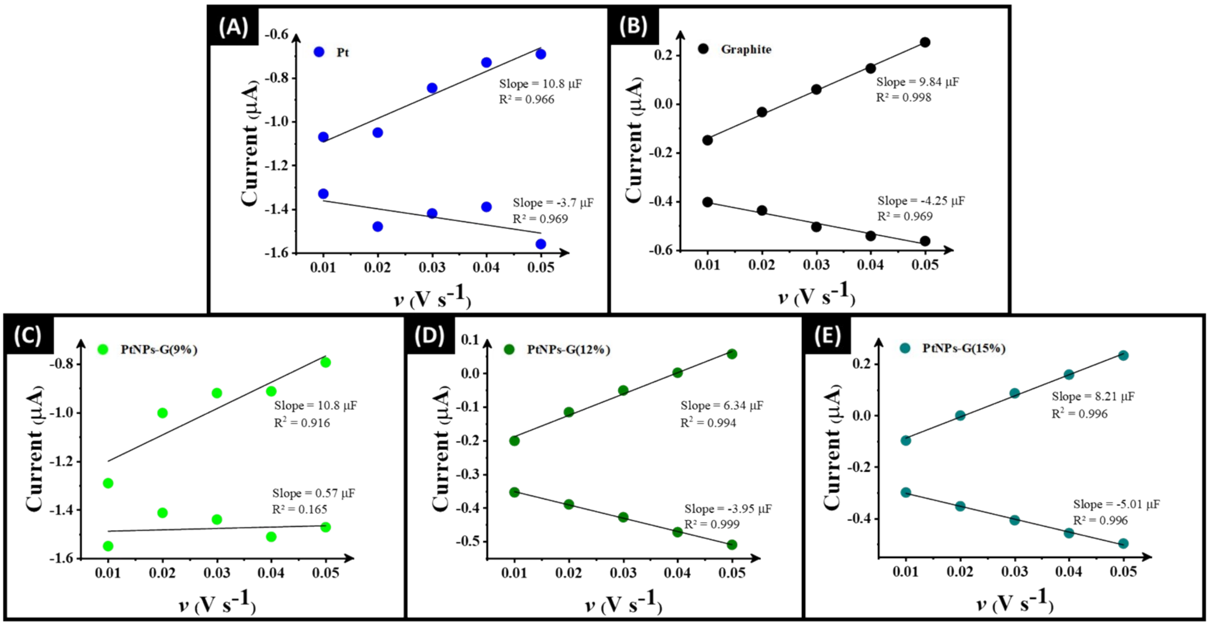

Figure S4. The cathodic and anodic charging currents measured at +0.20 V *vs* RHE as a function of scan rate (10 to 50 mV s^{-1}) in (A) polycrystalline platinum electrode, (B) Graphite and (C to E) electrodes with different amounts of PtNPs-G (9, 12, and 15%). The double-layer capacitance of the system is calculated as the average of the absolute values of the slopes of the linear fits to the data.

Table S1. Comparison of key performance parameters for the hydrogen evolution reaction across various catalysts

Electrode	Onset potential (mV)	η (mv)	Tafel (mV dec^{-1})	Ref
Mo_2TiC_2	−170	−379	50	1
Ti_3C_2	−330	−709	115	
Co_3O_4@Ni	−130	−225	65	2
PR-GDY/GC	–275	–475	75	3
Ni_2B/g-C_3N_4	300	707	221	4
$DPySc_3N@I_hC_{80}$	–25	—	115	5
$MoSe_2$/MXene	61	180	91	6
Pt/$C_{25\%}$-AME	–90	—	43	7
$M_{10\%}$–$C_{15\%}$ AME	–300	—	68	
PtNPs-G(12%) AME	–40	–0.312	46	This work

Key: Mo_2TiC_2 and Ti_3C_2: MXenes containing Mo–Ti (Mo_2TiC_2) and Ti (Ti_3C_2); Co_3O_4@Ni: three-dimensional (3D) urchin-like sphere arrays Co_3O_4 grown on Ni foam; PR-GDY/GC: pyrazine-incorporated graphdiyne nanofilm modified glassy carbon electrode; Ni_2B/g-C_3N_4: nickel boride (Ni_2B) nanoparticles incorporated into bulk graphitic carbon nitride (g-C_3N_4); $DPySc_3N@I_hC_{80}$: Diazonium functionalized fullerene with $Sc_3N@I_hC_8$; $MoSe_2$/MXene: $MoSe_2$/MXene MoSe2 grown in situ on the ultrathin titanium carbide substrate (MXene) generating a three-dimensional nanoflower; Pt/$C_{25\%}$ and $M_{10\%}$–$C_{15\%}$ AME: Additively manufactured electrodes with 25% of Pt/C commercially sourced carbon incorporate within the PLA filament and with 10% 2D-MoSe2 and 15% mass incorporation of Super P conductive carbon.

Table S2. Comparative synthesis methods highlighting the green chemistry advantages of the proposed PtNPs-G additive manufactured electrodes

Catalyst	Method	Solvent	Electrode	Ref
Mo_2TiC_2 and Ti_3C_2 (MXenes)	MXenes etched from MAX phases in 50 wt % HF (48 h, 45–55 °C), ultrasonicated (90 min), washed to pH 6, and dried at 80 °C.	HF and water	Glassy carbon disk	[1]
Co_3O_4@Ni	Co_3O_4@Ni synthesised via hydrothermal treatment (autoclave) of $Co(NO_3)_2$, urea, and HMTA in water (100 °C, 6 h) using HCl-cleaned Ni foam, followed by drying (60 °C) and annealing (250 ºC for 1h then 350 °C for 2h)	HCl and water	Ni foam	[2]
PR-GDY/GC	PR-GDY synthesised via liquid–liquid interfacial reaction using TIPS-TEP in o-dichlorobenzene and $[Cu(OH)TMEDA]_2Cl_2$ in ethylene glycol; TIPS group removed in situ with TBAF, reaction held at 40 °C for 2 d.	*o*-Dichlorobenzene and ethylene glycol	Glassy carbon electrode	[3]
Ni_2B/g-C_3N_4	g-C_3N_4 prepared by heating urea at 500 °C for 2 h in a semi-closed system. Ni_2B nanoparticles synthesized by redox	Water and ethanol	Glassy carbon electrode	[4]

Catalyst	Method	Solvent	Electrode	Ref
	reaction of $NiCl_2$ and $NaBH_4$, followed by mixing with g-C_3N_4 in ethanol and annealing at 500 °C for 2 h.			
$DPySc_3N@I_hC_{80}$	Py-NH_2-$Sc_3N@IhC_{80}$ reacted with HBF_4 in acetic acid/C_4S_2 (2:1) after sonication, followed by dropwise addition of isoamyl nitrite. Reaction stirred at room temperature for 50 min, then cooled to -20 °C for 20 h and washed with cooled diethyl ether to obtain $DPySc_3N@IhC_{80}$ (15% yield).	Acetic acid, isoamyl nitrite, and diethyl ether	Glassy carbon electrode	[5]
$MoSe_2$/MXene	Ammonium molybdate and SeO_2 were dissolved in MXene supernatant through ultrasonic treatment for 30 min, followed by the addition of ethanediamine and stirring (15 min). The mixture was heated (autoclave) at 200 °C for 20 h, then cooled to room temperature. The precipitates were collected, washed, dried, and annealed at	Ethanediamine, water and ethanol	Glassy carbon electrode	[6]

Catalyst	Method	Solvent	Electrode	Ref
	500 °C in N_2 for 1 h.			
$Pt/C_{25\%}$ and $M_{10\%}$–$C_{15\%}$	$MoSe_2$ was commercially obtained, and Pt/C refers to commercially sourced carbon supporting 20 wt% platinum.	Xylene and methanol	AME: 2D-$MoSe_2$ or Pt/C was dispersed in xylene and refluxed at 160 °C for 3 h, followed by the addition of PLA and electro-conductive carbon, and continued heating for 3 h. The mixture was recrystallised in methanol and dried at 50 °C until the xylene evaporated.	[7]
PtNPs-G	PtNPs were prepared onto graphite flakes by stirring graphite powder in an aqueous solution of platinum overnight. The resulting suspension containing PtNPs-graphite was then vacuum filtered and dried in an oven at 60 °C overnight.	Water	AME: recycled PLA, CB, PtNPs-G, and bio-based castor oil, using only 5 minutes of thermal mixing and no solvents.	This work

Key: HF: hydrofluoric acid; HMTA: hexamethylenetetramine; TIPS-TEP: triisopropylsilyl-protected tetraethynylpyrazine; $[Cu(OH)TMEDA]_2Cl_2$: di-µ-hydroxy-bis(N,N,N′,N′-tetramethylenediamine) copper(II); TBAF: tetrabutylammonium fluoride.

Physicochemical characterisation

X-ray Photoelectron Spectroscopy (XPS) data were acquired using an AXIS Supra (Kratos, UK) equipped with a monochromated Al X-ray source (1486.6 eV) operating at 225 W and a hemispherical sector analyzer. It was operated in fixed transmission mode with a pass energy of 160 eV for survey scans and 20 eV for region scans with the collimator operating in slot mode for an analysis area of approximately 700 × 300 μm, the full width at half maximum (FWHM) of the Ag $3d_{5/2}$ peak using a pass energy of 20 eV was 0.613 eV. Before analysis, each sample was ultrasonicated for 15 min in propan-2-ol and then dried for 2.5 hours at 65 °C as shown in our unpublished data to remove excess contamination and minimize the risk of misleading data. The binding energy scale was calibrated by setting the graphitic sp^2 C 1s peak to 284.5 eV; this calibration is acknowledged to be flawed [8] but was nonetheless used in the absence of reasonable alternatives, and because only limited information was to be inferred from absolute peak positions.

Scanning Electron Microscopy (SEM) micrographs were obtained using a Crossbeam 350 Focussed Ion Beam – Scanning Electron Microscope (FIB-SEM) (Carl Zeiss Ltd., Cambridge, UK) fitted with a field emission electron gun. Imaging was completed using a Secondary Electron Secondary Ion (SESI) detector. Samples were mounted on the aluminium SEM pin stubs (12 mm diameter, Agar Scientific, Essex, UK) using adhesive carbon tabs (12 mm diameter, Agar Scientific, Essex, UK) and coated with a 3 nm layer of Au/Pd metal using a Leica EM ACE200 coating system before imaging. EDX analysis on the samples was performed prior to sputtering.

X-ray diffraction (XRD) measurements were performed on the powder graphite samples to obtain the structural information using PANalytical X'Pert Powder X-ray diffractometer with Cu ($\lambda = 1.54$ Å) as the source with 45 kV voltage and 40 mA current settings. The data were collected in a continuous mode over the 2Θ scan range of 5° – 90°, with a step size of 0.01° for 108 seconds per step at room temperature under ambient conditions. The samples were spinning at 16 rpm during the measurements for uniform data collection. PreFIX module on the incident beam side with the automatic divergence and fixed anti-scatter slit of 4° along with PreFIX module on the diffracted side with PIXcel 1D detector in scanning line mode with programmable anti-scatter slit were used to collect the diffraction patterns from a constant irradiated length of 0.5 mm.

Electrochemical experiments

All electrochemical measurements were performed on an Autolab 100N potentiostat controlled by NOVA 2.1.7 (Utrecht, The Netherlands). The electrochemical characterization of the bespoke filament was performed using a lollipop design electrode (Ø5 mm disc with 8 mm connection length and 2 × 1 mm thickness [9]) alongside an external commercial Ag|AgCl (3M KCl) reference electrode with a nichrome wire counter electrode. All solutions of $[Ru(NH_3)_6]^{3+}$ were prepared using deionised water and were purged of O_2 thoroughly using N_2 prior to any electrochemical experiments. Solutions of $[Fe(CN)_6]^{4-}$ were prepared in the same way without the need of further degassing.

Electrochemical impedance spectroscopy (EIS) was recorded in the frequency range 0.1 Hz to 100 kHz, with 10 mV of signal amplitude applied to perturb the system under quiescent conditions. NOVA 2.1.7 software was used to fit Nyquist plots obtained to adequate equivalent circuit. Activation of the additive-manufactured electrodes was performed before electrochemical experiments using $[Fe(CN)_6]^{4-}$. This was achieved electrochemically in NaOH, as described in the literature [10]. Chronoamperometry was used to activate the additive-manufactured electrodes by applying a set voltage of +1.4 V for 200 s, followed by −1.0 V for 200 s. The additively manufactured electrodes were then thoroughly rinsed with deionised water and dried with compressed air before further use.

Double-layer capacitance data were obtained using cyclic voltammetry (CV) to assess the electrochemical active surface area (ECSA) of the additive manufactured electrodes used in this work for HER [11,12]. First, the potential range where there is a non-faradaic current response was determined from CV. Then, scan rate studies (0.010, 0.020, 0.030, 0.040, and 0.050 V s^{-1}) were performed across the non-faradaic region. In all experiments related to HER, a three-electrode system with a Reversible Hydrogen Electrode (RHE) reference (Gaskatel, Germany), a nichrome wire counter electrode, and a bespoke additive manufactured electrode as the working electrode was used and H_2SO_4 0.5 mol L^{-1} was used as supporting electrolyte. The use of a reversible hydrogen electrode (RHE) is a reference electrode, more specifically a subtype of the standard hydrogen electrodes, for electrochemical processes. Unlike the standard hydrogen electrode, its measured potential does change with the pH, so it can be used directly. The solution was purged of O_2 thoroughly using N_2 prior to any electrochemical experiments.

References

1 S. Delgado, Y. Remedios-Díaz, J. C. Calderón, S. Díaz-Coello, M. C. Arévalo, G. García and E. Pastor, *Int J Hydrogen Energy*, 2024, **55**, 1050–1061.

2 R. Li, D. Zhou, J. Luo, W. Xu, J. Li, S. Li, P. Cheng and D. Yuan, *J Power Sources*, 2017, **341**, 250–256.

3 R. Sakamoto, R. Shiotsuki, K. Wada, N. Fukui, H. Maeda, J. Komeda, R. Sekine, K. Harano and H. Nishihara, *J Mater Chem A Mater*, 2018, **6**, 22189–22194.

4 M. Cao, X. Zhang, J. Qin and R. Liu, *ACS Sustain Chem Eng*, 2018, **6**, 16198–16204.

5 O. Fernandez-Delgado, A. R. Puente Santiago, J. Galindo Betancourth, M. F. Sanad, S. T. Sreenivasan and L. Echegoyen, *Nanoscale*, 2022, **14**, 3858–3864.

6 J.-J. Huang, X.-Q. Liu, F.-F. Meng, L.-Q. He, J.-X. Wang, J.-C. Wu, X.-H. Lu, Y.-X. Tong and P.-P. Fang, *Journal of Electroanalytical Chemistry*, 2020, **856**, 113727.

7 J. P. Hughes, P. L. Dos Santos, M. P. Down, C. W. Foster, J. A. Bonacin, E. M. Keefe, S. J. Rowley-Neale and C. E. Banks, *Sustain Energy Fuels*, 2019, **4**, 302–311.

8 G. Greczynski and L. Hultman, *Scientific Reports 2021 11:1*, 2021, **11**, 1–5.

9 R. D. Crapnell, A. Garcia-Miranda Ferrari, M. J. Whittingham, E. Sigley, N. J. Hurst, E. M. Keefe and C. E. Banks, *Sensors 2022, Vol. 22, Page 9521*, 2022, **22**, 9521.

10 E. M. Richter, D. P. Rocha, R. M. Cardoso, E. M. Keefe, C. W. Foster, R. A. A. Munoz and C. E. Banks, *Anal Chem*, 2019, **91**, 12844–12851.

11 P. Connor, J. Schuch, B. Kaiser and W. Jaegermann, *Zeitschrift fur Physikalische Chemie*, 2020, **234**, 979–994.

12 C. C. L. McCrory, S. Jung, J. C. Peters and T. F. Jaramillo, *J Am Chem Soc*, 2013, **135**, 16977–16987.